Journal of Constructional Steel Research 65 (2009) 497–508

Contents lists available at ScienceDirect

Journal of Constructional Steel Research

journal homepage: www.elsevier.com/locate/jcsr

Analytical behavior of frames with steel beams to concrete-filled steel tubular column

Wen-Da Wang [a,b], Lin-Hai Han [b,*], Xiao-Ling Zhao [c]

[a] College of Civil Engineering, Lanzhou University of Technology, Lanzhou, 730050, China
[b] Department of Civil Engineering, Tsinghua University, Beijing, 100084, China
[c] Department of Civil Engineering, Monash University, Clayton, VIC 3168, Australia

ARTICLE INFO

Article history:
Received 11 March 2008
Accepted 2 November 2008

Keywords:
Concrete filled steel tubes
Column
Steel beam
Composite frame
Failure mode
Hysteretic model

ABSTRACT

This paper reports the mechanism of composite frames with steel beams connected to concrete-filled square hollow section (SHS) columns. Detailed analysis was carried out on longitudinal stress in steel beams, axial stress distribution in concrete, and concrete stress along the column height and at the connection panel. Parametric studies were conducted to investigate the influence of axial load level, beam-to-column linear stiffness ratio on the structural behavior of composite frames. Simplified hysteretic lateral load (P) versus lateral displacement (Δ) models are proposed for such composite frames.

© 2008 Elsevier Ltd. All rights reserved.

1. Introduction

Hollow structural steel (HSS) columns filled with concrete offer a number of benefits and are often used in tall buildings and other industrial structures. Concrete-filled steel tubular (CFST) columns are increasingly used in buildings due to their excellent static and seismic performance.

Chen et al. [1] presented different methods of advanced analysis for steel frames, such as elastic–plastic hinge method, refined plastic hinge method and plastic zone method. The analysis and design of composite frames with steel columns and steel–concrete composite beams under static loading were reported in Liew and Uy [2], Nethercot [3], Johnson [4], Li et al. [5,6]. The design of such composite frames under cyclic loading was reported in Plumier et al. [7], Bursi et al. [8], Thermou et al. [9]. CFST columns were not used in the above mentioned composite frames. Limited work was conducted on composite frames with CFST columns, as summarized in Hajjar [10] which also indicated the need to study mechanics models for such composite frames.

The authors have performed experimental investigation, as well as a finite element analysis (FEA) modeling on composite frames, consisting of steel beams and CFST columns [11]. This paper presents a detailed analysis on longitudinal stress in steel beams, axial stress distribution in concrete, and concrete stress along the column height and at the connection panel, by using the FEA modeling with ABAQUS [12]. Parametric studies are conducted to investigate the influence of axial load level and beam-to-column linear stiffness ratio on the structural behavior of composite frames. Simplified hysteretic lateral load (P) versus lateral displacement (Δ) models are proposed for such composite frames.

2. Stress analysis of the composite frame structures

2.1. General

A series of tests and FEA model on composite frames with steel beam to concrete-filled SHS steel tubular columns were conducted by the authors [11]. A typical frame specimen SF-22 [11] was selected to illustrate the mechanic model of the composite frames. The column in frame SF-22 is a concrete-filled SHS with a width of 140 mm and a thickness of 4 mm. The beam in frame SF-22 is an I-section with a flange width of 80 mm, a web depth of 180 mm and a thickness of 4.34 mm. In order to describe various stress distribution and deformation of the frames, five load stages were marked in the lateral load (P) versus lateral displacement (Δ) curves of the composite frame, as shown in Fig. 1.

The five points in Fig. 1 represent different stages during the incremental lateral load. Point one corresponds to the stage when the extreme fibers of the steel beam start to yield. Point two refers to the stage when the compression fibers of CFST steel columns reach their yield stress. Point three shows the ultimate lateral

* Corresponding author. Tel.: +86 10 62797067; fax: +86 10 62781488.
E-mail address: lhhan@tsinghua.edu.cn (L.-H. Han).

0143-974X/$ – see front matter © 2008 Elsevier Ltd. All rights reserved.
doi:10.1016/j.jcsr.2008.11.002

Nomenclature

E_c	Modulus of elasticity of concrete
E_s	Modulus of elasticity of steel
EI_c	Stiffness of CFST column
f'_c	Concrete cylinder compressive strength
f_t	Concrete tension strength
f_y	Yield strength of steel
i_b	Linear stiffness of steel beam for composite frame ($i_b = E_s I_b/L$)
i_c	Linear stiffness of CFST column for composite frame ($i_c = EI_c/L_c$)
I_b	Moment of inertia for steel beam
I_c	Moment of inertia for core concrete cross section
I_s	Moment of inertia for hollow steel cross section
k	Beam–column linear stiffness ratio
K_a	Stiffness in the elastic stage of composite frame for hysteretic model
K_T	Stiffness of the descending stage of composite frame for hysteretic model
k_m	Ultimate moment ratio between steel beam and CFST column of composite frame
L	The length of steel beam
L_c	Height of CFST column
M_{pc}	Ultimate moment of CFST column
n	Axial load level ($n = N/N_u$)
N	Axial load of CFST column
N_u	Ultimate compression resistance of CFST column
p	The hardening stage coefficient of moment versus curvature model for CFST column
P	Lateral load of frame
P_y	Ultimate lateral load capacity of composite frame in the hysteretic model
P_{yc}	Ultimate lateral load capacity of CFST column of composite frame in the hysteretic model
P_{max}	Ultimate lateral load capacity of frame
P_{ua}	Ultimate lateral load capacity of frame by ABAQUS
α	Steel ratio ($\alpha = A_s/A_c$)
σ	Stress
ε	Strain
Δ	Lateral displacement of frame
Δ_p	Lateral displacement when lateral load reaches P_y in the hysteretic model
Δ_u	Lateral displacement when lateral load of frame falls 85% of P_{max}
Δ_y	Yield displacement of frame
μ	Displacement ductility coefficient
μ_L	Effective length coefficient of CFST column

load (P_{max}) of the composite frame. Point four corresponds to the stage when the deflection reaches twice Δ_{max}. Point five is the stage when the load reaches 85% of the ultimate load P_{max}. Several sections in CFST columns and steel beam are selected (see Fig. 2) for stress analysis. Sections B1 and B2 are the plastic hinge locations in steel beam. Sections C1 and C2 are located at the bottom and top of the left CFST column. Section C1 is located near and outside of the stiffeners of columns, and section C2 is located under the steel beam. Sections C3 and C4 are the same as sections C1 and C2 except that they are located in the right column. Sections C5 and C6 are at the middle section of the left and right CFST column respectively, as shown in Fig. 2(a). Fig. 2(b) shows the deformation of the composite frame SF-22 at failure load. The four plastic hinges were located at the sections B1 and B2 in the steel beam and at sections C1 and C3 in the CFST columns. The deformation

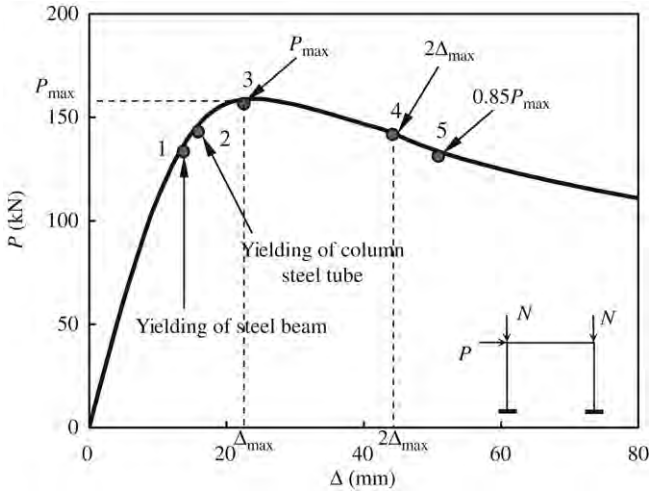

Fig. 1. Lateral load (P) versus displacement (Δ) curves of typical CFST frame SF-22 (Five Stages).

of the four plastic hinge sections at stage five, defined in Fig. 1, are shown in Fig. 3(a)–(d), respectively. The steel tubes of CFST columns at section C1 and C3 show evident outward buckling, whereas obvious local buckling occurs in the flanges and web of beam at section B1 and B2. The experimental result and FEA result by ABAQUS are consistent, as shown in Fig. 3.

2.2. Longitudinal stress in steel beams

Fig. 4 shows the longitudinal stress distribution of the steel beam of specimen SF-22 during the various load stages (e.g. one, three and five as defined in Fig. 1). The longitudinal tension and compression stress of section B1 and B2 were described as shown in Fig. 4(a)–(f). There was slight difference between the left beam end (B1) and the right beam end (B2). The beam was separated into two parts by a bending inflexion, and the two parts of the beam had different deformation curves. The inflexion was located approximately at the middle of the beam. The left part of the beam (B1) was in compression in the top flange and the upper web, and in tension in the bottom flange and the lower web. The right part of beam (B2) had the opposite sign. The plastic hinges were located near the ring plate. The compression and tension stress of steel beam were increasing with the incremental lateral load. The compression stress of flange at section B2 reached the yield stress. The yield area had extended from flange to web. When the composite frame reached its ultimate load (Stage three), about half of compression web in section B2 yielded. The tension area of web at section B2 did not yield at this stage. The lateral load began to descend from stage three, and local buckling appeared on the compressive web at section B2. The stress and deformation at section B1 were similar to section B2, but the stress value in section B1 was less than that in section B2, where the deformation of section B1 was smaller than that of section B2.

2.3. Concrete axial stress distribution

Fig. 5 shows the concrete axial stress distribution of section C1 of the composite frame SF-22 at the typical five load stages. f'_c is the cylinder compression strength of the concrete in the isoline. From Fig. 5, the axial stresses of concrete are different at various load stages. The section of CFST columns were compressed before the lateral load was applied. The tension area of the CFST square section appeared with the increasing of the lateral load. The tension area in concrete in CFST SHS columns extended, and the compression area decreased, with the incremental lateral

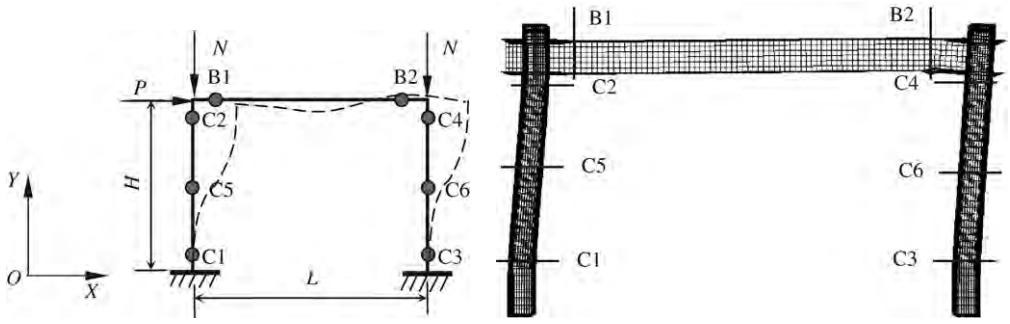

(a) Sections location of SF-22. (b) Deformation of SF-22 under failure mode (ABAQUS).

Fig. 2. Typical sections location of CFST composite frames SF-22.

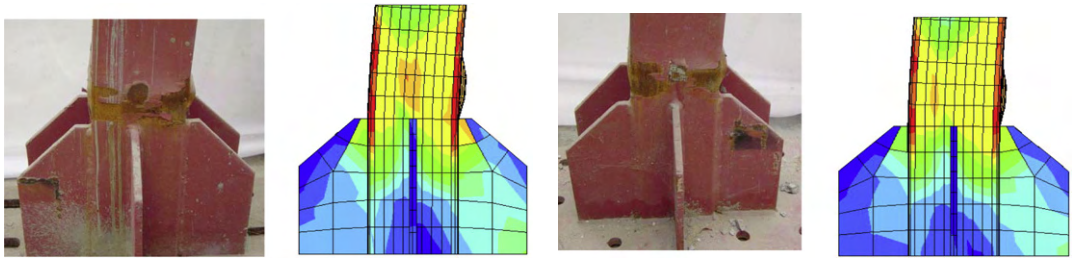

(a) Section C1. (b) Section C3.

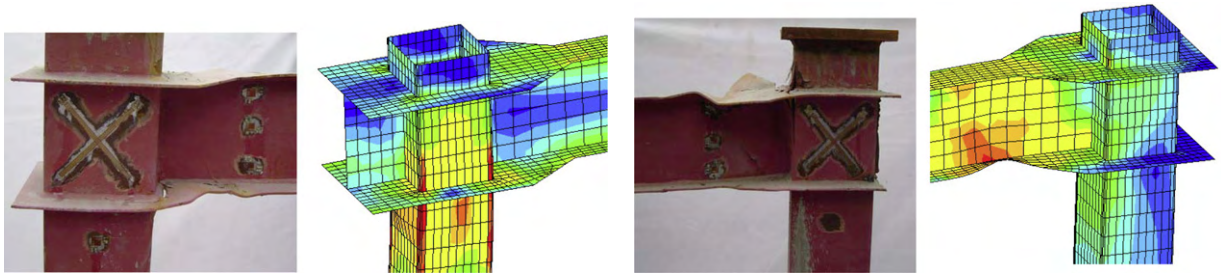

(c) Section B1. (d) Section B2.

Fig. 3. Comparison about the deformation at plastic hinge section between experiment and theory on CFST composite frame (SF-22).

load. The axial compression stress of core concrete in section C1 ascended with the incremental lateral load because of the bending moment effect. The concrete stress at the corner and flat zone were different, and the corner concrete stress of SHS CFST columns was much larger than the stress of the flat zone, as shown in Fig. 5. The corner concrete stress at compress zone reached $1.7f_c'$ and the value was $0.11f_c'$ in the central area at stage four. The corner concrete was confined by the tube much more effectively than other part of the concrete, so the stress was different. The stress concentration appeared in the corner concrete and the concrete near the stiffener plates. The boundary between tension and compress area on the section was approximately a straight line. The outside plane of SHS steel tube of CFST columns was in tension, and the inside plane of the columns was in compression. After the lateral load exceeded the ultimate load, local buckling appeared at the compression zone of steel tube of the columns and the stress decreased. The compression stress of steel tube reached yielded stress at stage two but tension stress was less than its yield stress. The reason was that the compression stress was a combination of axial compressive stress and bending stress. The local buckling appeared at compression zone of the steel tube at stage four and five, and the buckling went outward because the core concrete prevented the inward deformation. This means that the steel tube of CFST columns began to show local buckling after the lateral load began to descend. The core concrete offered effective support to the steel tube and delayed its local buckling. The stress states of section C3 were similar to that of section C1.

The CFST columns were subjected to combined axial compression forces and bending moment. Their deformation curves were anti-symmetric with a bending inflexion. Sections C5 and C6 were inverted moment points and the stresses at section C5 and C6 were expected to be lower. The concrete axial stress at section C5 and C6 at the ultimate load (Stage three) are shown in Fig. 6(a) (b), respectively. It can be seen that the concrete stress was tiny in general. The stress state at section C6 was barely different from the stress at section C5. This distinction is because the bending inflexions of the left and right CFST column are at different heights.

Sections C2 and C4 were located at CFST columns below the connection, and the concrete stress of sections C2 and C4 were similar to those of section C1 and C3 respectively, although the stress direction was reversed. The left area of sections C2 and C4 was the tension zone and the right area was the compression zone. The stress value at the same load stage of section C2 exceeded the stress of section C4, as shown in Fig. 7(a)–(f). The reason was that the lateral load of the right column was less than that of the left column. The tension area was increasing from stage one to stage five, and the compression area decreased for section C2 following the incremental lateral displacement.

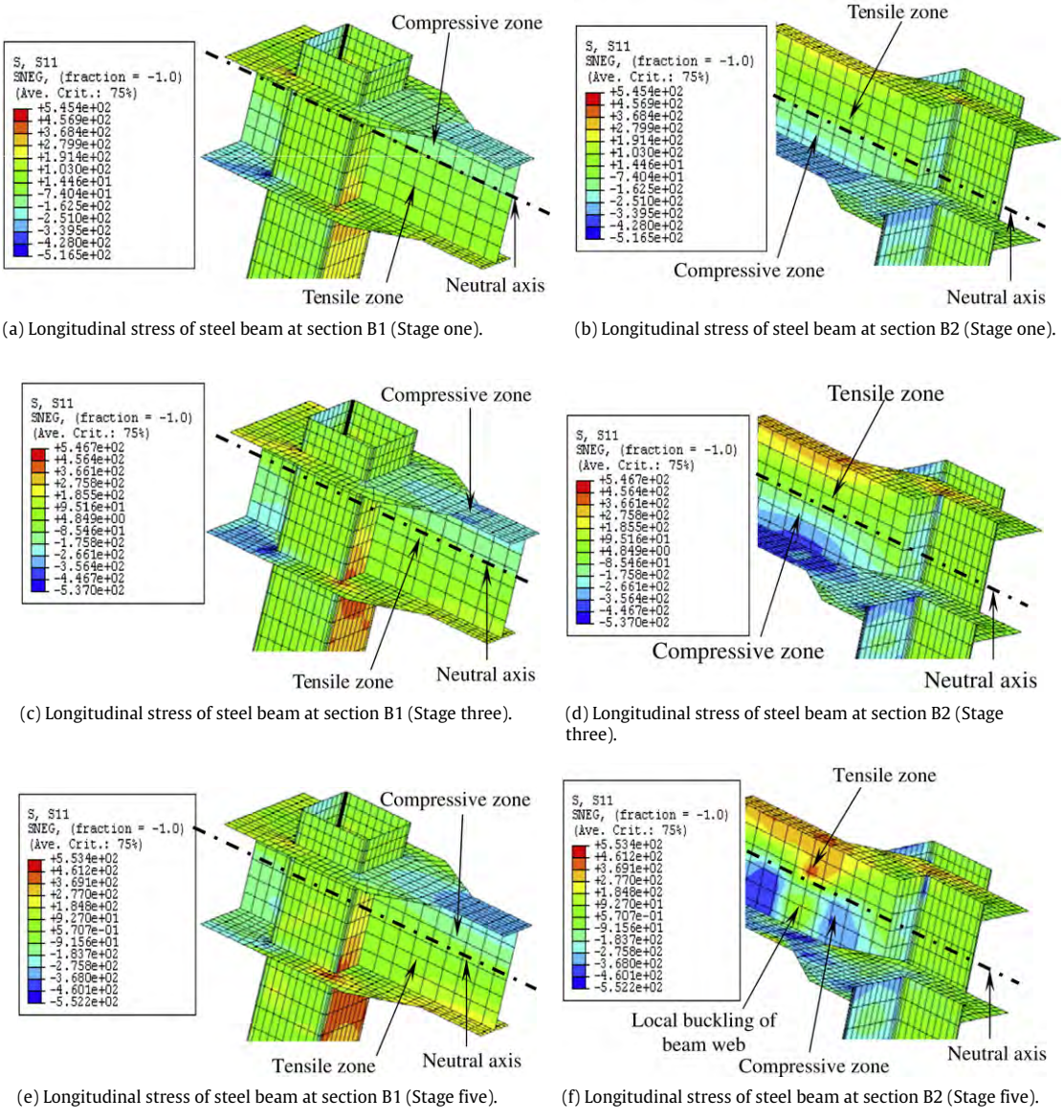

(a) Longitudinal stress of steel beam at section B1 (Stage one).

(b) Longitudinal stress of steel beam at section B2 (Stage one).

(c) Longitudinal stress of steel beam at section B1 (Stage three).

(d) Longitudinal stress of steel beam at section B2 (Stage three).

(e) Longitudinal stress of steel beam at section B1 (Stage five).

(f) Longitudinal stress of steel beam at section B2 (Stage five).

Fig. 4. Longitudinal stress of steel beam at the end section B1 and B2 under various lateral load stages.

2.4. Concrete stress along the column height

The concrete of CFST columns was cut to a section plane from the loading plane in order to show the concrete stress along the columns in the section plane under typical load stages, as shown in Fig. 8. The left and lower part of the columns were in tension. The right and upper part of the columns were in compression. The concrete axial stress and the tension area increased with the incremental lateral load. The stress distribution of the column was similar to that of the right column. The location of zero moment section in the right column was higher than that of the left column. The main reason is that the lateral top displacement of right column was transferred from the steel beam which also deformed.

2.5. Concrete stress at connection panel

In order to illustrate the core concrete stress of the composite joint panel in those composite frames, the core concrete stress distribution at connection panel under various loading were shown in Fig. 9(a)–(f). The stress value at the connection panel in the left columns was in general slightly larger than that of the right column under the same loading. Fig. 9 shows the different stress of core concrete in panel, and the left-bottom and right-top of core concrete in panel was compressive and the left-top and right-bottom of concrete was in tension. The tension and compression stresses were increased from stage one to stage three, decreased from stage four to stage five. It can be seen that all the axial compressive stress of core concrete except the local stress concentration zone, was less than the concrete cylinder compressive strength (f_c'). That means the connection strength exceeded that of the columns and beam for specimen SF-22. The plastic hinges of those frames were observed in the frame beam and columns.

3. Parametric analysis

Han et al. [13] analyzed the performance of concrete-filled thin-walled SHS and RHS beam–columns subjected to cyclic loading. It was shown that the axial load level (n is defined as N_o/N_u, where N_o is the axial load of the column and N_u is the axial compressive capacity of the column and N_u was determined by specification Eurocode 4 [14]), steel ratio (α is defined as

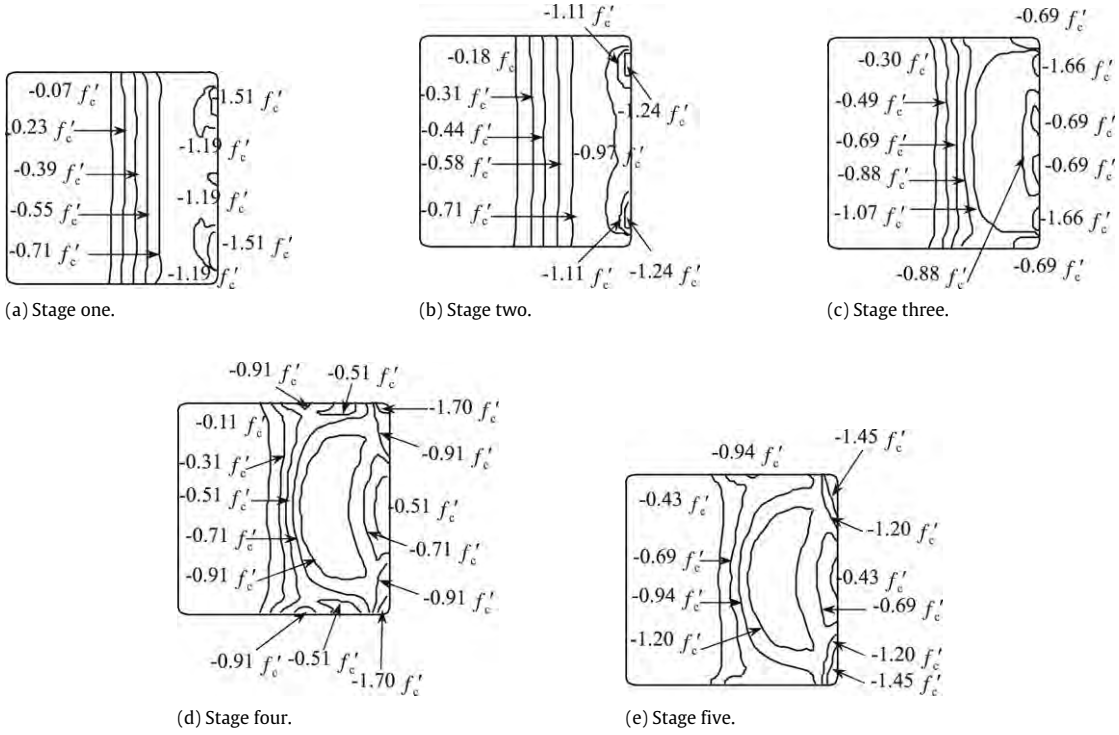

(a) Stage one. (b) Stage two. (c) Stage three.

(d) Stage four. (e) Stage five.

Fig. 5. Concrete axial stress distribution at section C1 of CFST frame (SF-22) columns under various lateral load stages.

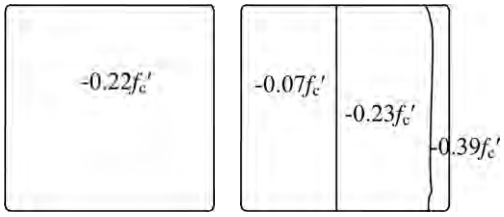

(a) Concrete stress at section C5 (Stage three). (b) Concrete stress at section C6 (Stage three).

Fig. 6. Concrete stress distribution at middle sections of SF-22 columns at ultimate strength point.

A_s/A_c, where A_s and A_c is the steel cross-sectional area of steel tube and core concrete, respectively), strength of steel (f_y) and concrete (f_{cu}), and column slenderness ratio (λ) are the main influential factors. The composite frame in this paper consisted of two CFST columns and one beam. The two columns act as beam–columns under combined axial force and lateral load. The steel beam provides certain restraints against the rotation and translation of columns. It also transfers the lateral load from one column to another. There are some differences between a single beam–column reported in Han et al. [13] and the columns in a composite frame because of the different boundary conditions. Thus, it is necessary to analyze the effect of different parameters on the behavior of such composite frame structure. The influence of those parameters on the composite CFST frames is expected to be similar to the CFST beam–columns, although the steel beam would affect the performance of composite frame. The beam to column linear stiffness ratio (k is defined as i_b/i_c, where i_b and i_c are linear stiffness of beam and column, respectively) can be an extra parameter to reflect the influence. Only the axial load level (n) and the beam to column linear stiffness ratio (k) are included in the parametric study in this paper, since the influence of other parameters ($\alpha, f_y, f_{cu}, \lambda$) are well known.

3.1. Effects of axial load level

3.1.1. Effects on concrete stress

Frames SF-11, SF-12 and SF-13 have the same column dimension and frame SF-21, SF-22 and SF-23 have the same column dimension as defined in Han et al. [11]. SF-22 based on Han et al. [11] was selected for the parametric study. Only sections C1 and C3 were selected for concrete stress analysis. Table 1 shows the maximum concrete axial stress value at section C1 and C3 of all composite frames under different load stages. The maximum compression stress is described in terms of the concrete cylinder compression strength (f_c') while the maximum tension stress is expressed in terms of the concrete tension strength (f_t). Most of the maximum compressive and tensile stresses are larger than the value of f_c' and f_t respectively. It reflects, to some extent, the improvement of core concrete strength due to the confinement of steel tubes. The core concrete axial stress distribution at section C1 of the composite frame specimens, SF-21, SF-22, SF-23, at ultimate load was shown in Fig. 10(a)–(c). The axial load levels varies from 0.04 to 0.6. Another analysis was conducted on a frame which has the same dimension as SF-22 with an axial load level of 0.9. (See Fig. 10(d).)

3.1.2. Effects on $P-\Delta/H$ curves

Fig. 11 shows the influence of axial load level (n) on the lateral load (P) versus the non-dimensional lateral displacement (Δ/H) relationship of the experimental composite frames. It can be found that the ultimate lateral load decreases with the increase of axial load level. The displacement ductility coefficient μ (μ is defined as Δ_u/Δ_y, where Δ_y is the lateral displacement at material yield and Δ_u is the lateral displacement when the lateral load falls to 85% of the maximum lateral strength P_{max}.) reduces from 0.6 to 0.04 with the increase of axial load level.

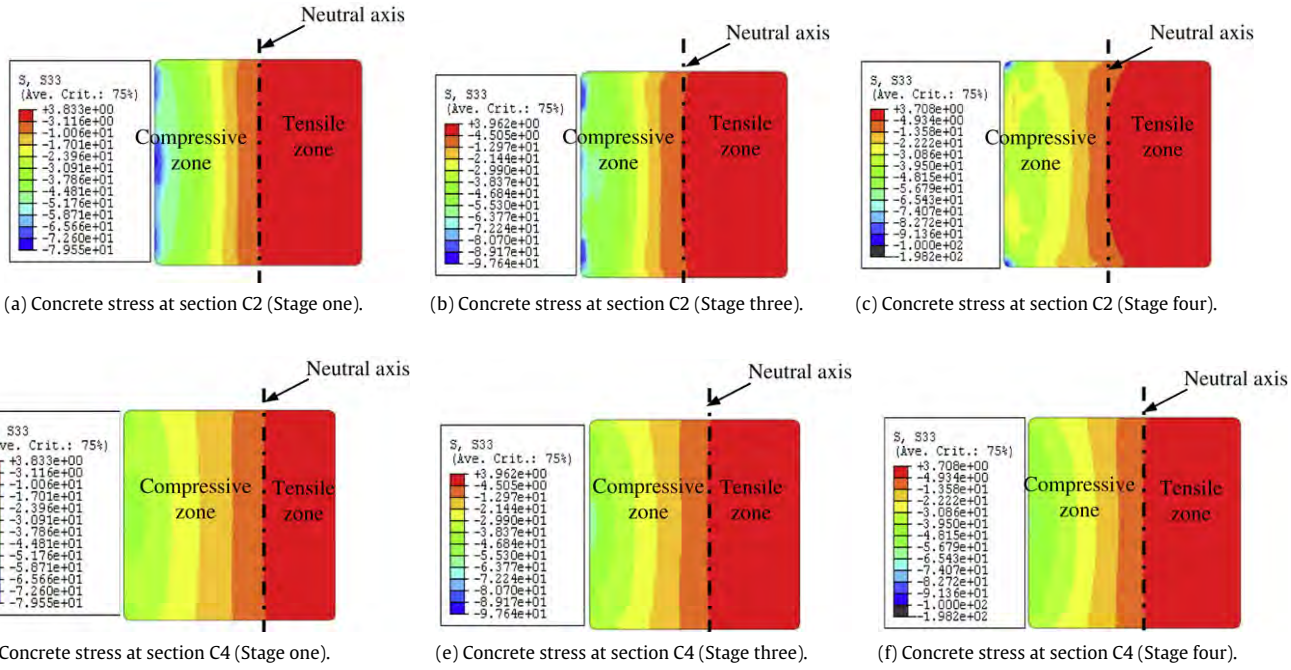

(a) Concrete stress at section C2 (Stage one).
(b) Concrete stress at section C2 (Stage three).
(c) Concrete stress at section C2 (Stage four).
(d) Concrete stress at section C4 (Stage one).
(e) Concrete stress at section C4 (Stage three).
(f) Concrete stress at section C4 (Stage four).

Fig. 7. Stress distribution at top sections of frame SF-22 columns at various lateral load stages.

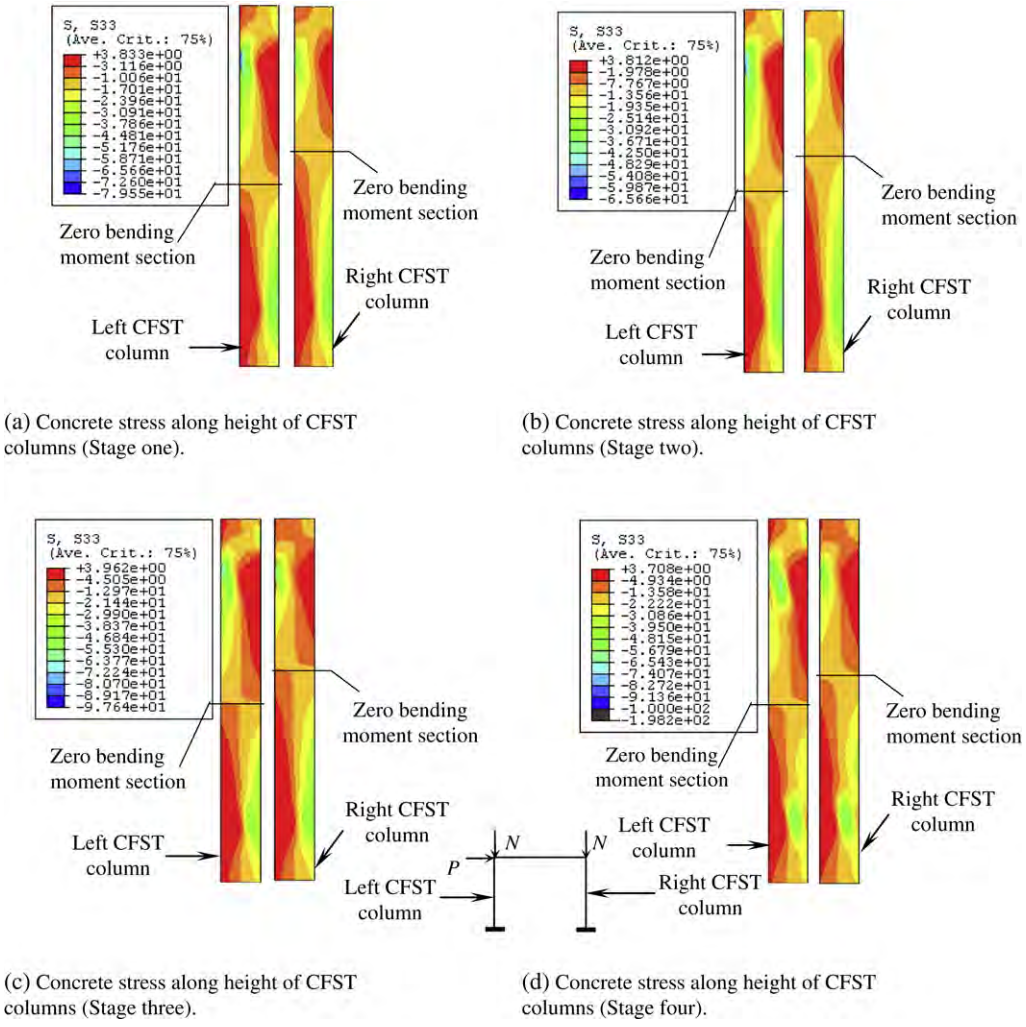

(a) Concrete stress along height of CFST columns (Stage one).
(b) Concrete stress along height of CFST columns (Stage two).
(c) Concrete stress along height of CFST columns (Stage three).
(d) Concrete stress along height of CFST columns (Stage four).

Fig. 8. Stress distribution of concrete along height of columns at various lateral load stages.

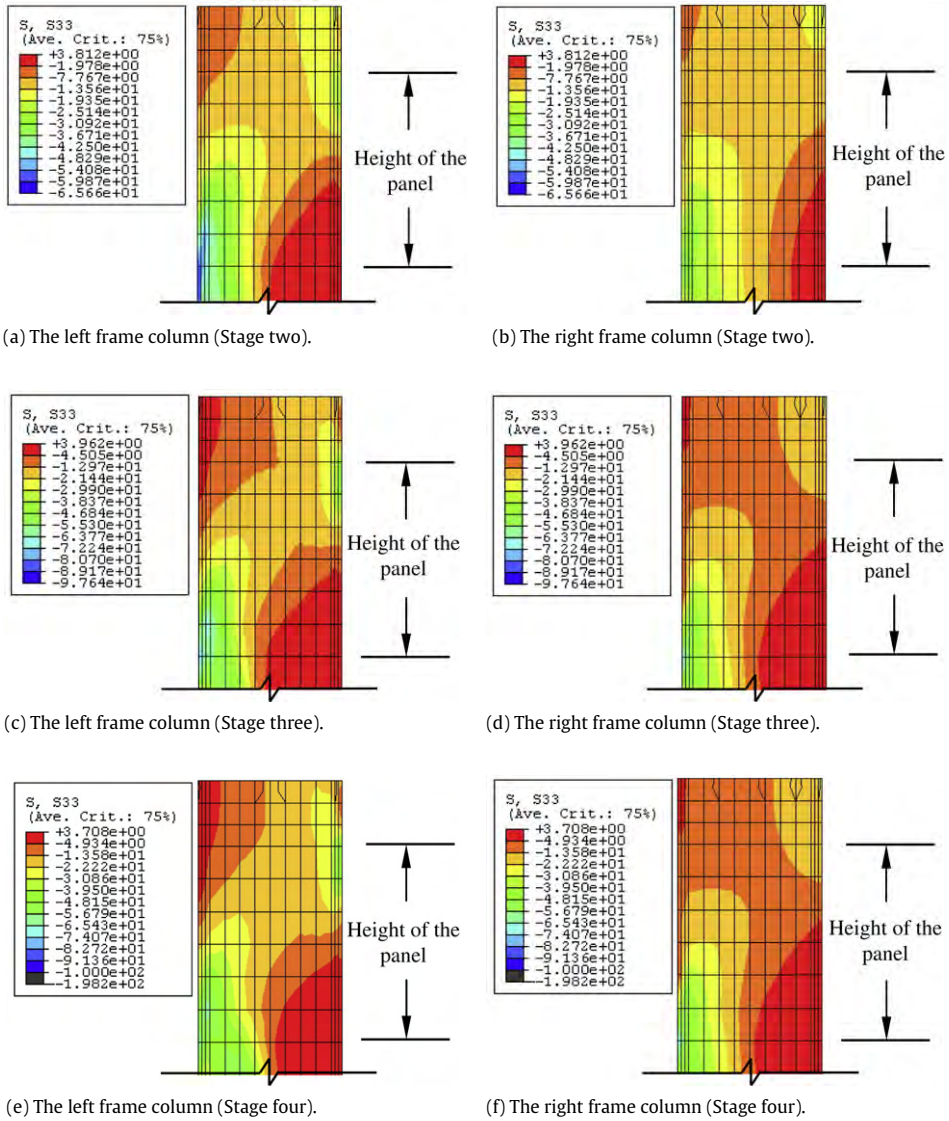

(a) The left frame column (Stage two).

(b) The right frame column (Stage two).

(c) The left frame column (Stage three).

(d) The right frame column (Stage three).

(e) The left frame column (Stage four).

(f) The right frame column (Stage four).

Fig. 9. Core concrete stress distribution at connection panel of composite frame SF-22 at various lateral load stages.

Table 1
Maximum concrete axial stress magnitude at section C1 and C3 of composite frames.

Axial load level n	Concrete axial stress maximum value at section C1 (MPa)				Concrete axial stress maximum value at section C3 (MPa)				Specimen
	Stage one	Stage two	Stage three	Stage four	Stage one	Stage two	Stage three	Stage four	
	$-0.83f_c'$[a]	$-1.04f_c'$	$-1.38f_c'$		$-0.70f_c'$	$-0.86f_c'$	$-1.40f_c'$		
0.05	$+1.13f_t$	$+1.07f_t$	$+1.00f_t$	*[b]	$+1.10f_t$	$+1.10f_t$	$+1.04f_t$	*[b]	SF-11
	$-1.23f_c'$	$-1.23f_c'$	$-1.61f_c'$	$-1.40f_c'$	$-1.04f_c'$	$-1.04f_c'$	$-1.52f_c'$	$-1.33f_c'$	
0.3	$+1.19f_t$	$+1.19f_t$	$+1.05f_t$	$+0.86f_t$	$+1.21f_t$	$+1.21f_t$	$+1.06f_t$	$+0.62f_t$	SF-12
	$-1.38f_c'$	$-1.24f_c'$	$-1.58f_c'$	$-1.35f_c'$	$-1.23f_c'$	$-1.08f_c'$	$-1.57f_c'$	$-1.47f_c'$	
0.6	$+1.12f_t$	$+1.10f_t$	$+1.04f_t$	$+0.86f_t$	$+1.09f_t$	$+0.69f_t$	$+1.09f_t$	$+0.89f_t$	SF-13
	$-0.98f_c'$	$-0.98f_c'$	$-1.73f_c'$		$-0.76f_c'$	$-0.76f_c'$	$-1.63f_c'$		
0.04	$+1.05f_t$	$+1.05f_t$	$+0.90f_t$	*[b]	$+1.12f_t$	$+1.12f_t$	$+0.93f_t$	*[b]	SF-21
	$-1.30f_c'$	$-1.14f_c'$	$-1.55f_c'$	$-1.12f_c'$	$-1.15f_c'$	$-1.01f_c'$	$-1.56f_c'$	$-1.08f_c'$	
0.3	$+1.31f_t$	$+1.35f_t$	$+1.22f_t$	$+1.04f_t$	$+1.33f_t$	$+1.33f_t$	$+1.26f_t$	$+0.99f_t$	SF-22
	$-1.24f_c'$	$-1.24f_c'$	$-1.46f_c'$	$-1.18f_c'$	$-1.14f_c'$	$-1.14f_c'$	$-1.44f_c'$	$-1.13f_c'$	
0.6	$+1.12f_t$	$+1.12f_t$	$+1.04f_t$	$+1.06f_t$	$+1.09f_t$	$+1.09f_t$	$+1.08f_t$	$+1.00f_t$	SF-23

[a] The symbol "+" means tension stress, and "−" means compression stress.
[b] The symbol "*" means the load versus displacement curves descend very slowly and the point four was non-existent.

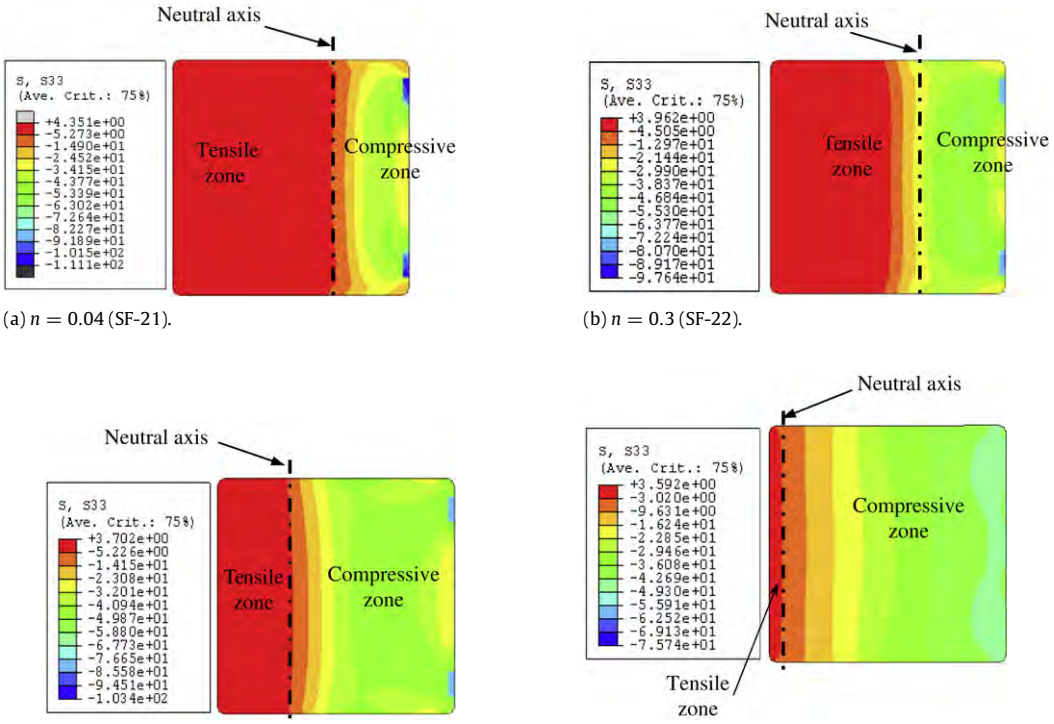

Fig. 10. Stress distribution of concrete at sections C1 of experimental CFST frames at ultimate load for various axial load level (n).

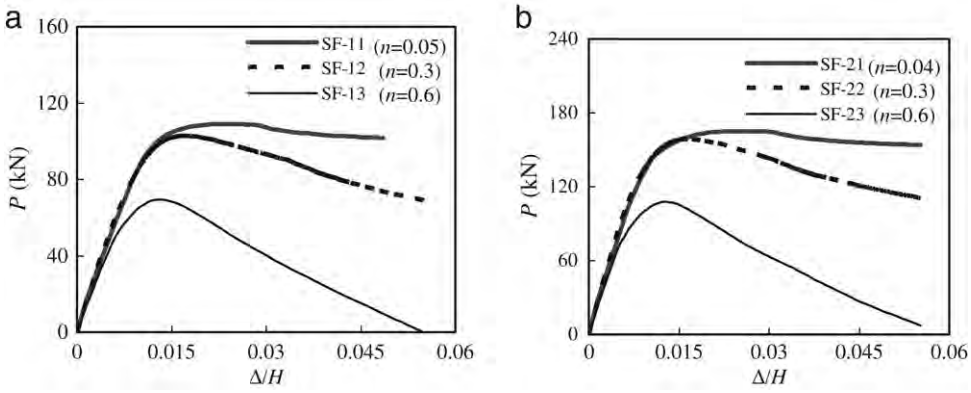

Fig. 11. Influence of axial load level (n) on P–Δ/H curves.

3.2. Effects of beam to column linear stiffness ratio

3.2.1. Effects on concrete stress

The basic dimension of a composite frame is the same as the specimen SF-22. The beam size is changed in order to form a different beam to column linear stiffness ratio. Fig. 12 shows the effect of k on the concrete stress of CFST columns at section C1. The analysis examples were given in two types of beam to column linear stiffness ratios under the same axial load level. The beam to column linear stiffness ratio ranges from 0.34 to 0.62, with the axial load level being 0.3 or 0.6, respectively. It seems that k value does not affect the concrete stress distribution, although the stress magnitude was slightly different by comparing Fig. 12(a) and (b) and by comparing Fig. 12(d) and (e).

3.3. Effects on P–Δ/H curves

The lateral load (P) versus the non-dimensional displacement (Δ/H) curves of the typical composite frames was given in Fig. 12(c) and (f) respectively. It is shown that the lateral ultimate load of the frame increases as the incremental ratio increases. The constraint of columns from the beam would be enhanced for a larger beam to column linear stiffness ratio, hence an increase in ultimate load of frame.

4. Simplified model P–Δ hysteretic relationship

4.1. Typical lateral load (P) versus lateral displacement (Δ) relationship

Fig. 13 shows typical lateral load (P) versus lateral displacement (Δ) relationships of the composite frames (e.g. SF-22). The characteristics of the curve are shown below.

Elastic stage (from point O to point A): The yielding of steel beam's flange occurs at point A.

Elastic–plastic stage (from point A to point B): The steel section starts to yield and the yielding area of the compression zone of CFST columns gradually increases, which leads to the gradual reduction

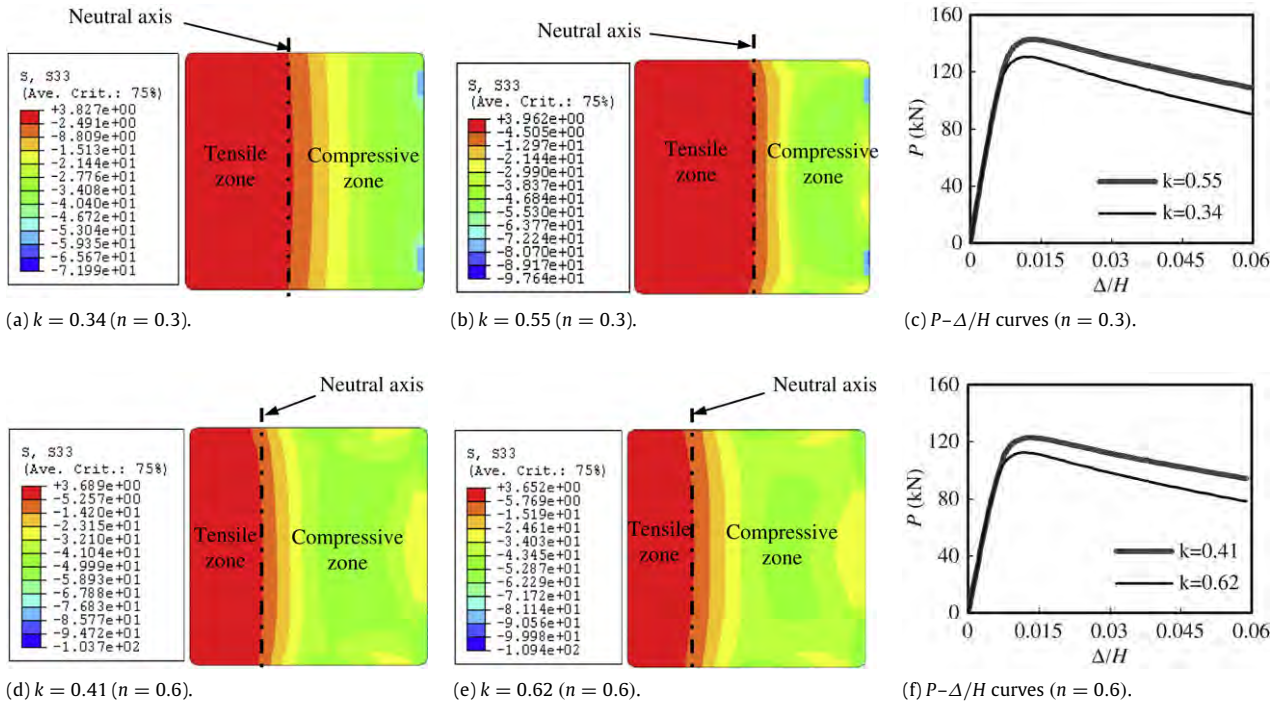

Fig. 12. Influence of beam to column linear stiffness ratio (k) on concrete stress and P–Δ/H curves.

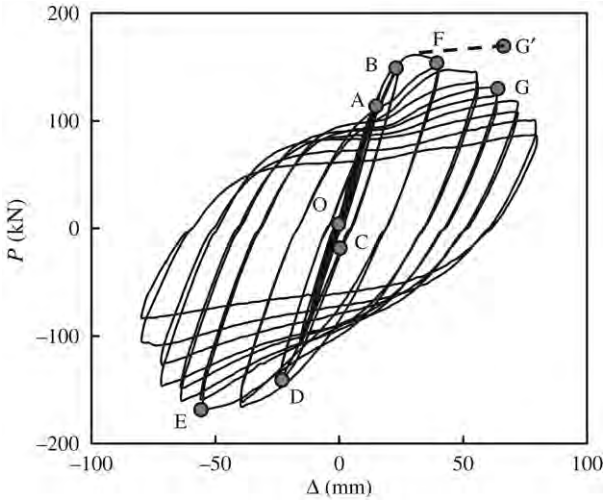

Fig. 13. Typical lateral load (P) versus lateral displacement (Δ) curve of composite frame SF-22.

in stiffness. The shape of the curve mainly depends on the value of axial load level (n). When n is small (e.g. less than 0.3), the curve goes up steadily to point B. When n is high, the curve starts to go down after a short increase to point B. The smaller the axial load level, the later the curve starts to descend.

Unloading stage (from point B to point C): The load (P) versus displacement (Δ) curve generally shows a linear behavior.

Elastic–plastic stage of reverse loading (from point C to point D): The load (P) versus displacement (Δ) relationship shows nonlinear behavior. The stiffness of the columns decreases with the increase of the yielding zone in the steel beam and CFST column bottom, as well as the tensile zone in the cross sections of the composite columns.

Strengthening stage (from point D to point E or from B to F): During this stage, the sectional stiffness of the steel beam or CFST column is very small. The load increases slowly but the deformation increases quickly.

Re-loading stage (from point E to point F): The load (P) versus displacement (Δ) curve shows similar behavior as the stage from point B to point C, D and E.

Strengthening stage (from point F to point G′) or descending stage (from point F to point G): When the value of axial load level (n) is small (e.g. less than 0.3), the curve (FG′) goes up steadily, similar to stage BF. When n is high, the curve (FG) starts to go down.

4.2. Simplified second-order analysis on lateral load (P) versus lateral displacement (Δ) relationship of composite frame

The second-order elastic–plastic analysis method (Chen et al. [1]) consists of two different models, namely the concentrated-plastic method (or so called second-order elastic–plastic hinge model, Liew et al. [2]), and the spread-plastic method (or so called plastic zone model). The FEM model in this paper is based on the plastic zone model to simulate composite CFST frame. A simplified second-order inelastic analysis on lateral load (P) versus lateral displacement (Δ) relationship of composite frame is proposed to assist designers.

It was found from the parameters analysis in Section 3 that the main influential factors for lateral load (P) versus lateral displacement (Δ) relationships of the composite frames were the axial load level (n), steel ratio (α), strength of steel (f_y) and concrete (f_{cu}), column slenderness ratio (λ), and the beam to column linear stiffness ratio (k). Generally, the envelope of the P–Δ cyclic curves can be simplified and expressed by a tri-linear model, as shown in Fig. 14. The line OA represents the elastic stage, and the lines AB and BC represent the elastic–plastic stage and descending stage. Different methods were used in the three different stages. The second-order elastic analysis was used in the elastic stage. The second-order plastic hinge analysis was used in the elastic–plastic stage. The descending stage was simulated using rigid-plastic analysis. The analysis procedures were similar to those described in Chen et al. [1]. The plastic hinges were formed at the beam end and the column bottom of the composite frame in the elastic–plastic stage. The plastic hinges of the beam were firstly formed. The simplified second-order inelastic analysis depends

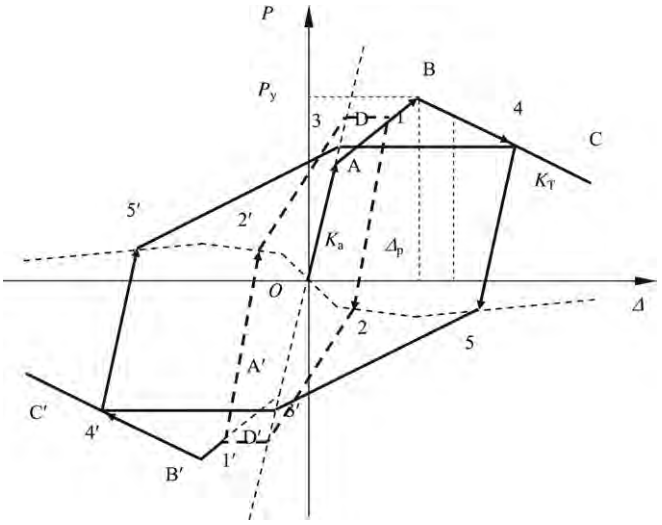

Fig. 14. A schematic view of simplified lateral load (P) versus lateral deflection (Δ) relationship.

on the following four key parameters for the hysteretic lateral load (P) versus lateral displacement (Δ) relationship of composite frame: stiffness in the elastic stage (K_a) of composite frame, the ultimate strength (P_y) and corresponding displacement (Δ_p), and the stiffness of the descending stage (K_T).

4.3. Simplified hysteretic model of lateral load (P) versus lateral displacement (Δ) relationship

The simplified hysteretic lateral load (P) versus lateral displacement (Δ) models for the CFST beam–columns in Han et al. [13] is modified to simulate the behavior of the composite frame, i.e. the model parameters are obtained from the composite frame. The key parameters (K_a, P_y, Δ_p, K_T) are defined from the simplified second-order inelastic analysis mentioned above.

(1) Stiffness in the elastic stage (K_a) of the composite frame is given by

$$K_a = 2\left(\frac{12i_c}{L_c^2} - \frac{6N}{5L_c}\right) - 2\frac{\left(\frac{6i_c}{L_c} - \frac{N}{10}\right)^2}{4i_c + 3i_b - \frac{2NL_c}{15}} \tag{1}$$

where i_c and i_b is the linear stiffness of CFST column and steel beam respectively, L_c is the height of column, N is the axial force in the column. i_c is defined as EI_c/L_c, where L_c is the height of column. The stiffness of concrete filled SHS column is $EI_c = E_sI_s + 0.2E_cI_c$ given in AIJ [15], where E_s and E_c are modulus of elasticity of steel and concrete, respectively, and I_s and I_c are moment of inertia for hollow steel cross section and core concrete cross section, respectively. i_b is defined as E_sI_b/L, where I_b is moment of inertia for steel beam, E_s is the modulus of elasticity of steel and L is the beam length.

(2) The ultimate strength (P_y) of composite frame is given by

$$P_y = 2P_{yc} \tag{2}$$

where P_{yc} is the ultimate lateral load capacity of CFST beam–columns, which can be determined using a design code for composite structures. The predicted values of P_{yc} based on different design codes do not vary significantly. In this paper Eurocode 4 [14] is adopted as an example. Modification of the effective length coefficient is necessary, due to the influence of the steel beam which provides certain restraints against end rotation of the columns. The modified effective length coefficient μ_L of the CFST column is similar to that given in [16].

$$\mu_L = \sqrt{\frac{3.75i_b/i_c + 4}{3.75i_b/i_c + 1}} \tag{3}$$

where i_c and i_b is the linear stiffness of CFST column and steel beam respectively.

(3) The corresponding displacement (Δ_p) is given by

$$\Delta_P = \Delta_A + \frac{\left(4i_c - \frac{2NL_c}{15} + 3i_b\right)}{\left(\frac{6i_c}{L_c} - \frac{N}{10}\right)}\frac{k_mM_{pc}}{3i_b} + \frac{4i_c - \frac{2NL_c}{15}}{\left(\frac{12i_c}{L_c^2} - \frac{6N}{5L_c}\right)\left(4i_c - \frac{2NL_c}{15}\right) - \left(\frac{6i_c}{L_c} - \frac{N}{10}\right)^2} \times \left(\frac{M_{pc} - M_{1c}}{L_c}\right) \tag{4}$$

where Δ_A is the elasticity displacement of the composite frame, and $\Delta_A = 0.6P_y/K_a$. M_{pc} is ultimate moment of CFST column, and can be determined based on Eurocode 4 [14]. k_m is the ratio between the ultimate moment of steel beam to CFST column. The parameter M_{1c} is given by

$$M_{1c} = \left(-\frac{6i_c}{L_c} + \frac{N}{10}\right) \cdot \frac{\left(4i_c - \frac{2NL_c}{15} + 3i_b\right)}{\left(\frac{6i_c}{L_c} - \frac{N}{10}\right)}\frac{k_mM_{pc}}{3i_b} + \left(2i_c + \frac{NL_c}{30}\right) \cdot \frac{k_mM_{pc}}{3i_b}. \tag{5}$$

(4) The stiffness of the descending stage (K_T) of composite frame is given

$$K_T = 2\left(p\left(\frac{12EI_c}{L_c^3} - \frac{6N}{5L_c}\right) - \frac{p\left(\frac{6EI_c}{L_c^2} - \frac{N}{10}\right)^2}{\frac{4EI_c}{L_c} - \frac{2NL_c}{15}} - (1-p)\frac{N}{L_c}\right) \tag{6}$$

where EI_c is the stiffness of CFST column. p is the hardening stage coefficient of moment versus curvature model for CFST SHS column and is given by Han et al. [13]. The other parameters are the same as defined above.

The composite frame consists of the CFST columns and steel beam. The unloading stage and re-loading stage of the frame was decided mainly by the performance of the CFST columns. So the unloading and re-loading stage of CFST columns from Han et al. [13] can be used to simulate the same load stage on the composite frame. The lateral loads at point 2 and point 2′ (shown in Fig. 14) are given by $0.2P_1$ and $-0.2P_1$, respectively. The lateral loads at point 5 and point 5′ (shown in Fig. 14) are given by $0.2P_4$ and $-0.2P_4$, respectively. The validity ranges of this simplified model are: $n = 0$–0.8, $\alpha = 0.03$–0.2, $\lambda = 10$–80, $f_y = 200$–500 MPa, $f_{cu} = 30$–80 MPa and $\xi = 0.2$–4. In general, the above values are typical in practice.

The steps to calculate the P–Δ hysteretic curve based on the simplified model can be summarized as follows:

(1) To calculate the values of K_a, P_y, Δ_p, K_T and the coordinates of point A and B in Fig. 14;

(2) To initialize a displacement increment with a value of an increment of 10% of yield displacement Δ_y.

(3) If the displacement is less than Δ_A, to determinate the corresponding load P according to the line OA. The load P should be calculated from line AB if the displacement is between Δ_A and Δ_B. If the displacement is greater than Δ_B, the load should be descended from line BC. This is similar if the displacement is negative.

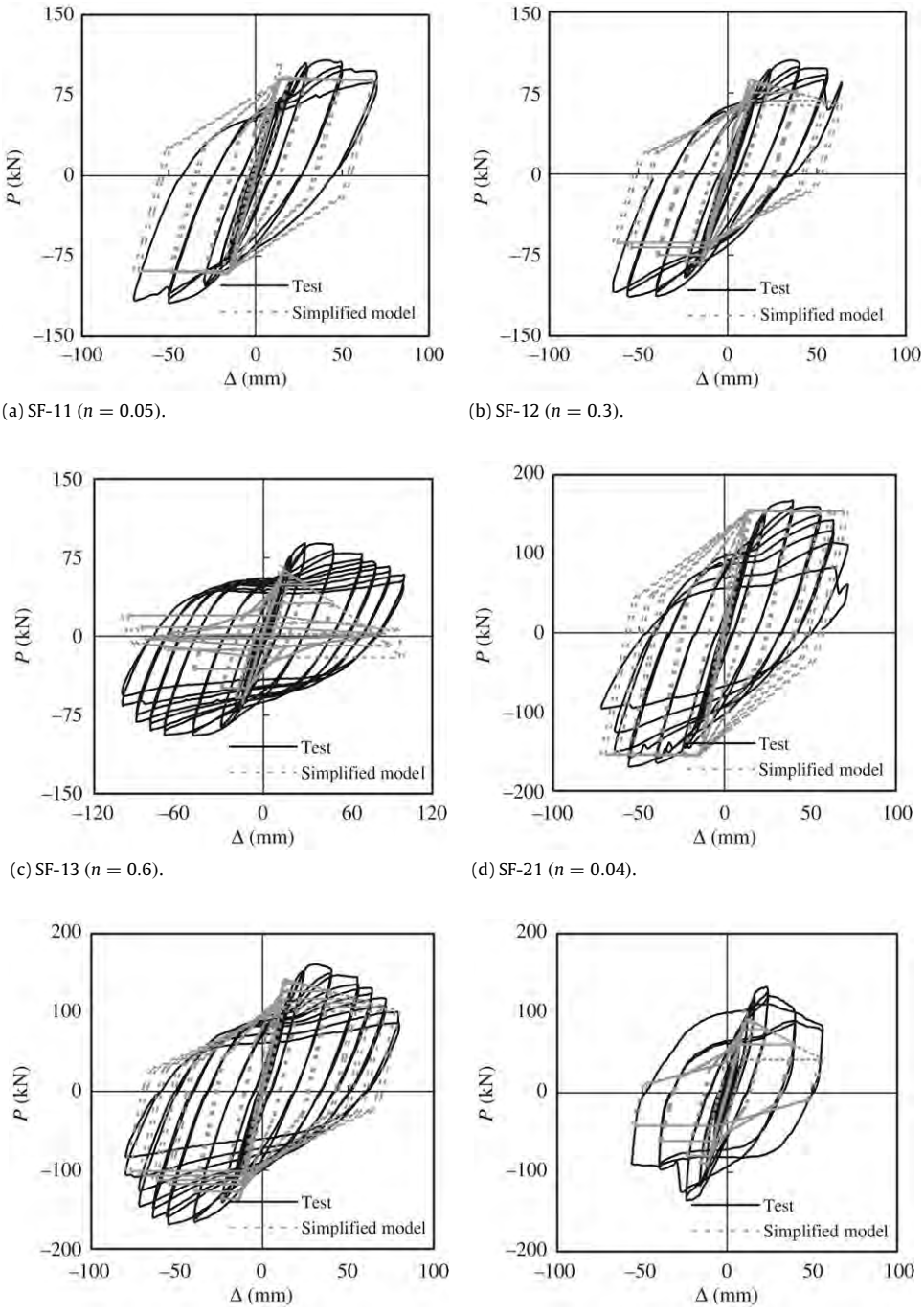

(a) SF-11 ($n = 0.05$). (b) SF-12 ($n = 0.3$).

(c) SF-13 ($n = 0.6$). (d) SF-21 ($n = 0.04$).

(e) SF-22 ($n = 0.3$). (f) SF-23 ($n = 0.6$).

Fig. 15. Comparison of calculated lateral load (P) versus lateral deflection (Δ) hysteretic relationships between simplified model and the experimental results.

(4) If the former displacement increment is positive, it means the loading stage. Otherwise it means the unloading stage. The load is calculated by corresponding loading stage or unload stages.

(5) Repeat step (2)–(4) until the displacement reaches its desired value.

To verify the simplified model, the predicted P–Δ hysteretic relationship using the simplified model are compared in Fig. 15 with experimental curves from Han et al. [11]. It can be found from the comparisons, that a reasonable agreement is achieved.

5. Conclusions

From the results of this paper, the following conclusions may be drawn within the limitations of the analysis:

(1) Detailed analysis was carried out on longitudinal stress in steel beams, axial stress distribution in concrete, and concrete stress along the column height and at the connection panel. The steel tubes and core concrete of the composite frames illustrated good mechanical performance because of the composite action.

(2) Parametric studies showed that the axial load level in the column and beam to column linear stiffness ratio were key factors for performance of the composite frames. The other parameters have a similar effect on the frames as on single beam–column.

(3) A simplified hysteretic lateral load (P) versus lateral displacement (Δ) models were proposed for such composite

frames, based on parametric studies. The simplified $P-\Delta$ models agreed well with the experimental results. The model is useful in dynamic analysis for concrete filled steel tubular structures.

Acknowledgments

The research reported in the paper are the Projects supported by Specialized Research Fund for the Doctoral Program of Higher Education (SRFDP) (20070003087), and part of Project 50425823 supported by National Natural Science Foundation of China. Their financial support is highly appreciated.

References

[1] Chen WF, Toma S. Advanced analysis for steel frames: Theory, software and applications. Boca Raton (Florida): CRC Press; 1994.
[2] Liew JYR, Uy B. Advanced analysis of composite frames. Progress in Structural Engineering and Materials 2001;3(2):159–69.
[3] Nethercot DA. Composite construction. London (NY): Spon Press; 2003.
[4] Johnson RP. Composite structures of steel and concrete: Beams, slabs, columns, and frames for buildings. third ed. Malden: Blackwell Publishing; 2004.
[5] Li TQ, Moore DB, Nethercot DA, Choo BS. The experimental behaviour of a full-scale, semi-rigidly connected composite frame: Overall considerations. Journal of Constructional Steel Research 1996;39(3):167–91.
[6] Li TQ, Moore DB, Nethercot DA, Choo BS. The experimental behaviour of a full-scale, semi-rigidly connected composite frame: Detailed appraisal. Journal of Constructional Steel Research 1996;39(3):193–220.
[7] Plumier A, Schleich JB. Seismic resistance of steel and composite frame structures. Journal of Constructional Steel Research 1993;27(1–3):159–76.
[8] Bursi OS, Sun FF, Postal S. Non-linear analysis of steel–concrete composite frames with full and partial shear connection subjected to seismic loads. Journal of Constructional Steel Research 2005;61(1):67–92.
[9] Thermou GE, Elnashai AS, Plumier A, Doneux C. Seismic design and performance of composite frames. Journal of Constructional Steel Research 2004;60(1):31–57.
[10] Hajjar JF. Composite steel and concrete structural systems for seismic engineering. Journal of Constructional Steel Research 2002;58(5–8):703–23.
[11] Han LH, Wang WD, Zhao XL. Behaviour of steel beam to concrete-filled steel tubular column frames: Finite element model and verifications. Engineering Structures 2008;30(6):1647–58.
[12] Hibbitt, Karlson & Sorensen Inc. ABAQUS/standard User's Manual. Version 6.5. Hibbitt, Karlsson, & Sorensen, Inc. Providence (RI); 2005.
[13] Han LH, Yang YF, Tao Z. Concrete-filled thin-walled steel SHS and RHS beam–columns subjected to cyclic loading. Thin-Walled Structures 2003; 41(9):801–33.
[14] Eurocode 4. Design of composite steel and concrete structures-Part 1.1 General rules and rules for buildings. Brussels (Belgium): European Committee for Standardization. BS EN 1994-1-1; 2004.
[15] AIJ. Recommendations for design and construction of concrete filled steel tubular structures. Architectural Institute of Japan (AIJ). Tokyo (Japan); 1997 [in Japanese].
[16] Ballio G, Mazzolani FM. Theory and design of steel structures. London/New York: Chapman and Hall; 1983.